Slow Inactivation Differs Among Mutant Na Channels Associated with Myotonia and Periodic Paralysis

Lawrence J. Hayward,* Robert H. Brown, Jr.,* and Stephen C. Cannon*§
*Department of Neurology, Massachusetts General Hospital, and §Department of Neurobiology, Harvard Medical School, Boston, Massachusetts 02114 USA

ABSTRACT Several heritable forms of myotonia and hyperkalemic periodic paralysis (HyperPP) are caused by missense mutations in the α subunit of the skeletal muscle Na channel (SkM1). These mutations impair fast inactivation or shift activation toward hyperpolarized potentials, inducing persistent Na currents that may cause muscle depolarization, myotonia, and onset of weakness. It has been proposed that the aberrant Na current and resulting weakness will be sustained only if Na channel slow inactivation is also impaired. We therefore measured slow inactivation for wild-type and five mutant Na channels constructed in the rat skeletal muscle isoform (rSkM1) and expressed in HEK cells. Two common HyperPP mutations (T698M in domain II-S5 and M1585V in IV-S6) had defective slow inactivation. This defect reduced use-dependent inhibition of Na currents elicited during 50-Hz stimulation. A rare HyperPP mutation (M1353V in IV-S1) and mutations within the domain III–IV linker that cause myotonia (G1299E) or myotonia plus weakness (T1306M) did not impair slow inactivation. We also observed that slow inactivation of wild-type rSkM1 was incomplete; therefore it is possible that stable membrane depolarization and subsequent muscle weakness may be caused solely by defects in fast inactivation or activation. Model simulations showed that abnormal slow inactivation, although not required for expression of a paralytic phenotype, may accentuate muscle membrane depolarization, paralysis, and sensitivity to hyperkalemia.

INTRODUCTION

Missense mutations in the α subunit of the skeletal muscle Na channel (SkM1) cause several heritable forms of myotonia or periodic paralysis (reviewed in Cannon, 1996). As a first step toward understanding the pathophysiological basis for the aberrant electrical excitability of skeletal muscle in these disorders, the functional consequences of mutations in SkM1 have been studied in cultured myotubes (Cannon et al., 1991, 1995; Lerche et al., 1993; Tahmoush et al., 1994; Lerche et al., 1996) and in heterologous expression systems (Cannon and Strittmatter, 1993; Cummins et al., 1993; Chahine et al., 1994; Mitrovic et al., 1994, 1995; Yang et al., 1994; Hayward et al., 1996). For each of the 12 mutations characterized in these studies, the most common functional defect is a disruption of fast inactivation. Mutant channels have a combination of slowed rates of inactivation, shifts in steady-state inactivation, faster rates of recovery from inactivation, and increased persistent current at the end of a 50-ms depolarization. Two mutations, T704M and G1306E, also cause a hyperpolarized shift in the voltage dependence of activation. In model simulations of a muscle cell (Cannon et al., 1993; Cannon, 1994a; Hayward et al., 1996), these functional defects in the fast gating of SkM1 are sufficient to cause the repetitive discharges that give rise to myotonia and to depolarize the cell; this depolarization inactivates the majority of Na channels and thereby causes failure of spike generation and weakness.

A much slower form of voltage-dependent inactivation, on a time scale of seconds to minutes, is a fundamental property shared by all Na channels (Rudy, 1978; Almers et al., 1983; Simoncini and Stühmer, 1987). Slow inactivation is kinetically distinct from fast inactivation, and the two are structurally dissociated as well. Treatment with internal proteases (Rudy, 1978) or mutations in the III–IV linker that disable fast inactivation (Cummins and Sigworth, 1996; Featherstone et al., 1996) do not impair slow inactivation.

Ruff (1994) proposed that a defect of slow inactivation must also occur in SkM1 mutations that cause periodic paralysis. Muscle depolarization and weakness in hyperkalemic periodic paralysis (HyperPP) may last for several hours. Although the defects identified in the fast inactivation of mutant Na channels can produce depolarization of the resting potential (Cannon et al., 1993), Ruff argued that within a few minutes, slow inactivation would shut off the aberrant Na current and the muscle would repolarize. In view of the fact that 1) the integrity of slow inactivation had not been examined in SkM1 mutants, 2) knowledge of the fast gating defects was not sufficient to predict the effects on slow inactivation, and 3) model simulations implied that even with intact slow inactivation weakness could occur (Cannon, 1994b), testing of Ruff's proposal had to await direct measurement of slow inactivation in mutant channels. Cummins and Sigworth (1996) found that slow inactivation was disrupted in rT698M, the rat homolog of the most common mutation associated with HyperPP, hT704M, in human SkM1. Even after a 15-min depolarization to −20

Received for publication 10 September 1996 and in final form 10 December 1996.

Address reprint requests to Dr. Stephen C. Cannon, EDR 413A, Massachusetts General Hospital, Boston, MA 02114. Tel.: 617-724-3531; Fax: 617-726-5256; E-mail: cannon@helix.mgh.harvard.edu.

0006-3495/97/03/1204/16 $2.00

mV, ~25% of the maximum Na current recovered within 10 ms at −100 mV. In comparison, less than 3% of the current recovered for wild-type channels.

We have characterized slow inactivation in rat SkM1 mutants corresponding to five disease-associated mutations of human SkM1. Two mutations (T698M and M1585V, residues numbered according to the rat cDNA) cause HyperPP with severe episodic weakness as the predominant symptom, and a third (M1353V) causes a variant of HyperPP with muscle stiffness in addition to weakness. The G1299E mutation causes a form of sodium channel myotonia (SCM) associated with severe myotonia but no paralysis (Lerche et al., 1993). The final mutation tested, T1306M, corresponds to the most frequent mutation found in families with paramyotonia congenita (PMC). Myotonia, aggravated by cold or repetitive motion, is the presenting symptom in PMC, although weakness can occur with extreme cooling. We found that the two most common HyperPP mutants (T698M and M1585V), but not the rarer variant (M1353V), had impaired slow inactivation. Slow inactivation was preserved for the PMC (T1306M) and SCM (G1299E) mutations. Our data indicate that a defect of slow inactivation, although not a requirement for the expression of a paralytic phenotype, may accentuate muscle membrane depolarization, muscle paralysis, and sensitivity to hyperkalemia.

MATERIALS AND METHODS

Expression of sodium channels

We previously subcloned the WT rat skeletal muscle Na channel α subunit cDNA (rSkM1, μl; Trimmer et al., 1989) into the *Eco*RI site of the mammalian expression vector pRC/CMV (Invitrogen) and generated a 503-bp *Cla*I-*Sac*II mutagenesis cassette spanning the domain III–IV linker to IV-S4 (bases 3865 to 4367) (Hayward et al., 1996). The construction of point mutations rG1299E and rT1306M within the III–IV linker, corresponding to the human disease mutations hG1306E and hT1313M, was described by Hayward et al. (1996). The same method of polymerase chain reaction (PCR) overlap extension from the cassette template was used to generate the rM1353V mutant (homolog of hM1360V in domain IV-S1) for the present study. The mutagenic fragment was ligated into the expression construct and verified by sequencing the cassette and flanking regions. The mutants rT698M and rM1585V (corresponding to hT704M in domain II-S5 and hM1592V in IV-S6) were previously described by Cannon and Strittmatter (1993). The human β_1 subunit cDNA (McClatchey et al., 1993) was subcloned into the *Eco*RI site of the mammalian expression vector pcDNAI (Invitrogen).

HEK cells were cultured as described previously (Hayward et al., 1996). Plasmid DNAs encoding wild-type or mutant rat Na channel α subunits (0.25 μg or 0.03 pmol/35-mm dish), the human Na channel β_1 subunit (fourfold molar excess over α subunit DNA), and a CD8 marker (0.1 μg) were cotransfected into HEK cells by the calcium phosphate method (Sambrook et al., 1989). At 2–4 days after transfection, the HEK cells were trypsinized briefly and passaged to 35-mm dishes for electrophysiological recording. Individual transfection-positive cells were identified with >90% efficiency by affinity for 4.5 μm-diameter microbeads coated with anti-CD8 antibody (Dynal, Great Neck, NY; Jurman et al., 1994).

Whole-cell recording

Whole-cell Na currents were measured with an Axopatch 200A amplifier (Axon Instruments, Foster City, CA). The amplifier output was filtered at 5 kHz and digitally sampled at 50 kHz using an LM900 interface (Dagan, Minneapolis, MN). Data was stored to a 486-based computer under the control of a custom Axobasic data acquisition program.

Several criteria were used to define acceptable conditions for recording Na currents. To minimize the contribution of endogenous currents to the records, cells with peak currents of <1 nA upon step depolarization from −120 to −10 mV were excluded. Conversely, cells with peak currents of >20 nA were excluded to minimize peak voltage errors due to series resistance. The average cell capacitance was 23 ± 8 pF (range 9–43 pF, n = 50), and the average uncompensated series resistance was 3.0 ± 0.9 MΩ (range 1.2–5.4 MΩ, n = 50). The series resistance was compensated by the analog circuitry of the amplifier (>90% according to the dial), and thus the predicted time constant for the voltage clamp was 7 μs and the estimated peak voltage error was 2.3 ± 1.7 mV (range 0.09–6.3 mV, n = 50). In practice, residual capacitance transients indicated a clamp settling time of ~100 μs. Leakage conductance was corrected by digital scaling and subtraction of passive currents elicited by depolarization from −120 to −90 mV. Whole-cell resistance was required to be >0.5 GΩ and averaged 2.9 GΩ. Shifts in the voltage dependence of gating and variations in peak current are often observed during whole-cell recording. To minimize these effects, we waited an average of ~12 min for equilibration after gaining access to the cell, and then measured slow inactivation. The peak amplitude and decay time constant of the current elicited by the conditioning pulses (−120 to −10 mV) in prolonged pulse protocols were monitored to verify that gating kinetics remained stationary and that channels fully recovered between trials. Cells were rejected from the analysis if these features changed by more than 10%.

Patch electrodes were fabricated from borosilicate capillary tubes (1.65 mm O.D.) with a two-stage puller (Sutter, Novato, CA). The shank of the pipette was coated with Sylgard, and the tip was heat polished to a final diameter of 0.5–2.0 μm. The pipette solution contained (in mM): 105 CsF, 35 NaCl, 10 EGTA, and 10 Cs-HEPES (pH 7.4). Fluoride was used in the pipette to prolong seal stability. The bath contained 140 NaCl, 4 KCl, 2 $CaCl_2$, 1 $MgCl_2$, 5 glucose, and 10 Na-HEPES (pH 7.4). Recordings were made at room temperature (21–23°C).

Data analysis and modeling

Curve fitting was performed manually off-line using AxoBasic, SigmaPlot (Jandel Scientific, San Rafael, CA), or Origin (Microcal, Northhampton, MA). Conductance was calculated as $G(V) = I_{peak}(V)/(V - E_{rev})$, where the reversal potential E_{rev} was measured experimentally for each cell. Steady-state fast and slow inactivation was fitted to a Boltzmann with a nonzero pedestal, I_o, calculated as $I/I_{peak} = [1 - I_o]/[1 + \exp((V - V_{1/2})/k)] + I_o$, where $V_{1/2}$ is the half-maximum voltage, and k is the slope factor (Table 1). Symbols with error bars indicate means ± SEM, and parameter values represent means ± SD. Statistical significance was determined by the unpaired t-test with p values noted in the text.

The model proposed by Cannon et al. (1993) was used to simulate the electrical excitability of a muscle cell. Parameters for activation and fast inactivation of wild-type Na channels were modified to match the properties of rSkM1 expressed in HEK cells (Hayward et al., 1996). A slow inactivation variable, $s(V, t)$, with intrinsic voltage and time dependence, was added to our previous model, as described in the Discussion.

RESULTS

Fast inactivation

The kinetics of Na channel gating were characterized by recording whole-cell currents from HEK cells transiently transfected with cDNAs encoding either wild-type (WT) or mutant rSkM1, the rat skeletal muscle isoform of the α subunit. In all experiments, cells were cotransfected with a human β_1 subunit cDNA. Defects in fast gating have been

TABLE 1 Parameter estimates for inactivation of Na channels at 22°C

		Fast inactivation, h_∞ (V)		Slow inactivation, s_∞ (V)		
Disease	Mutation	$V_{1/2}$ (mV)	k (mV/e-fold)	$V_{1/2}$ (mV)	k (mV/e-fold)	$\bar{s}$
Normal	Wild-type	−66.7 ± 4.0 (11)	4.6 ± 0.2	−61.6 ± 4.2 (8)	10.8 ± 1.3	0.099 ± 0.017
HyperPP	T698M	−70.8 ± 4.4 (14)	4.8 ± 0.5	−34.0 ± 4.4 (6)*	24.7 ± 2.3*	0.300 ± 0.017*
HyperPP	M1585V	−66.7 ± 4.2 (9)	5.0 ± 0.5	−49.9 ± 6.9 (7)*	15.3 ± 1.4*	0.162 ± 0.036*
HyperPP	M1353V	−69.0 ± 3.1 (6)	5.5 ± 0.3*	−61.5 ± 6.7 (4)	11.1 ± 1.3	0.073 ± 0.003
SCM	G1299E	−57.8 ± 3.0 (6)*	4.3 ± 0.4	−53.2 ± 5.7 (5)	9.8 ± 1.7	0.086 ± 0.018
PMC	T1306M	−49.3 ± 4.2 (5)*	4.4 ± 0.3	−62.6 ± 6.3 (3)	6.8 ± 0.3*	0.080 ± 0.005

Values are mean ± SD (n).
*Significant difference compared to WT ($p < 0.001$).

reported previously for each mutant in this study (Cannon and Strittmatter, 1993; Cummins et al., 1993; Mitrovic et al., 1995; and Hayward et al., 1996), except M1353V, which had not yet been tested. The most prominent changes caused by M1353V were a 50% increase in the persistent current measured 50 ms after a step to −10 mV (see legend, Fig. 10) and a twofold increase in the time constant for the macroscopic current decay, τ_h, at test potentials of > −20 mV (data not shown).

The voltage dependence of steady-state fast inactivation was examined more extensively, because discrepancies have been reported for the relative midpoints of fast and slow inactivation for SkM1 expressed in HEK cells (Cummins and Sigworth, 1996) or oocytes (Featherstone et al., 1996) as compared to native Na channels in skeletal muscle (Almers et al., 1983; Ruff et al., 1987; Simoncini and Stühmer, 1987). The voltage dependence of fast inactivation was measured at a series of conditioning pulse durations to establish a minimum interval that was sufficiently long for fast inactivation to reach steady state at 22°C. Cells were held at −120 mV, a conditioning pulse of defined duration and voltage was applied, the membrane was stepped to −80 mV for 0.2 ms to deactivate channels, and peak I_{Na} was measured at a test depolarization of −10 mV. Peak currents were normalized to the maximum value recorded from a conditioning pulse of −140 mV. The voltage dependence of Na channel availability (fraction not fast-inactivated) shifted in the hyperpolarizing direction and became steeper

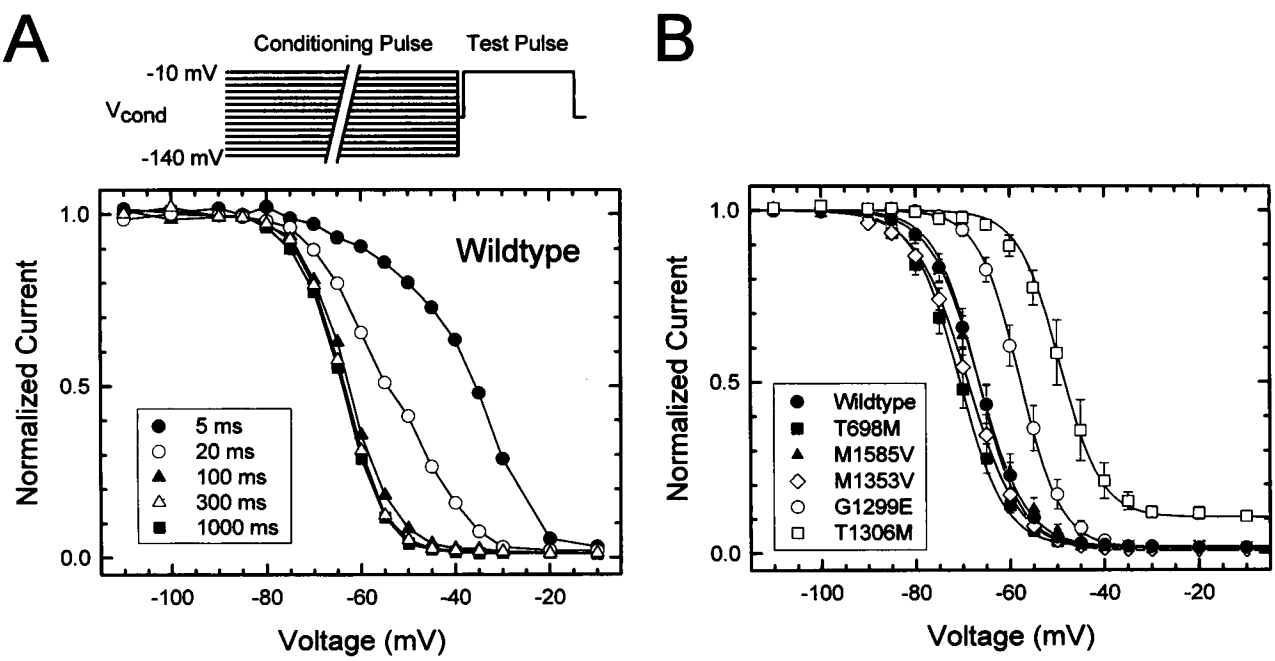

FIGURE 1 Voltage dependence of fast inactivation. (*A*) Channel availability was measured as the peak Na current elicited by depolarization to −10 mV, after a conditioning pulse at potentials of −140 to −10 mV. Amplitude was normalized to the current after a conditioning pulse at −140 mV. After completion of the sequence of conditioning potentials, the duration of the conditioning pulse was changed and the sequence was repeated. The inset shows a schematic of the pulse protocol, which included a 0.2-ms gap to −80 mV to deactivate channels before application of the test pulse. Membrane potential was returned to a holding potential of −100 mV for 3 s between trials. For this representative wild-type cell, inactivation during the conditioning pulse did not reach equilibrium for durations less than 100 ms. (*B*) The voltage dependence of steady-state fast inactivation was measured using the same protocol as in *A* and a fixed 300-ms conditioning pulse. Curves show fits to a Boltzmann function (plus a constant value of 0.10 for T1306M); parameter values and number of cells are listed in Table 1. Symbols depict the means ± SEM.

for progressively longer conditioning pulse durations. The shift approached a limiting value for conditioning pulse durations of 100 ms or greater (Fig. 1 *A*). Each mutant was also tested with the series of conditioning durations used in Fig. 1 *A*, and the leftward shift in availability always saturated by 100 ms (data not shown). When briefer conditioning pulses were applied, the availability curves were shifted in the depolarized direction and were not well fitted by a simple Boltzmann function, because channels did not have sufficient time to equilibrate between closed and fast-inactivated states. Thus 300 ms was used as conservative estimate of the time required for fast inactivation to reach steady state over a voltage range of −140 to −10 mV.

The voltage dependence of steady-state fast inactivation, $h_\infty(V)$, measured with a 300-ms conditioning pulse, is shown for WT and each of the five mutants in Fig. 1 *B*. The data were fitted with a Boltzmann function (plus a constant term), and the parameter values are listed in Table 1. Mutations associated with prominent myotonia (G1299E and T1306M) caused a rightward (depolarized) shift in the midpoint ($p < 0.001$), whereas those associated with HyperPP (T698M, M1585V, M1353V) did not. The nonzero pedestal of $h_\infty(V)$ for T1306M after large depolarizations (> -30 mV) occurred because ~10% of channels failed to inactivate, even after 300 ms.

The pathophysiological significance of altered fast gating for mutant Na channels is uncertain over long time periods (seconds to minutes), especially since the "persistent" I_{Na} and "steady-state" inactivation were measured with voltage steps lasting less than 1 s. Bursts of myotonia last for seconds, and attacks of depolarization-induced weakness may continue for hours or even days. Prolonged depolarization, however, reduces the availability of Na channels over a time scale of seconds to minutes. This slow inactivation process could attenuate aberrant Na currents produced by fast inactivation defects and thereby profoundly influence the excitability of affected muscle. It has been postulated that slow inactivation of mutant Na channels must be disrupted to produce the prolonged depolarization that occurs in affected muscle (Ruff, 1994). To test this hypothesis, we measured slow inactivation for WT and each mutant Na channel.

T698M and M1585V mutations disrupted slow inactivation

Because both fast- and slow-inactivated channels are nonconducting, a brief hyperpolarizing pulse is employed to distinguish between the occupancy of these two states. During the brief hyperpolarization, fast-inactivated channels ideally recover completely to resting closed states, whereas the recovery of slow-inactivated channels is negligible. The Na current elicited after a brief hyperpolarization, therefore, reflects the fraction of channels that are not slow inactivated.

Fig. 2 shows the relative Na current availability recorded from WT and mutant channels as the holding potential was stepped, every few minutes, over a range of −100 to +20 mV. Sodium currents were measured every 15 s by using the sequence of pulses diagrammed in Fig. 2. A 20-ms prepulse to −100 mV was applied to allow recovery from fast inactivation. Next, the peak Na current was measured during a 3-ms depolarization to −10 mV. This test pulse was followed by a series of four voltage steps from −120 (2 ms) to −90 mV (3 ms) to measure the passive leakage current, and then the voltage was reset to the holding potential. Comparison of the left panels in Fig. 2, *A* and *C*, shows a defect of slow inactivation for T698M channels. Depolarization to −10 mV caused a 90% reduction in available current from WT channels, whereas at the same holding potential only about 60% of T698M channels were slow inactivated. Conversely for M1353V mutants, which also cause HyperPP, channels slow inactivated to the same extent as WT channels: ≥90% at −10 mV and ~60% at −60 mV (Fig. 2 *B*).

The kinetics of entry to and recovery from slow inactivation were complex, consisting of multiple exponential components. The data in Fig. 2 show that a rapid component(s) of slow inactivation, accounting for about 80% of the response, was too fast to be resolved with sampling every 15 s. At the other extreme, slow components continued to relax over several minutes. The slow relaxations in Na channel availability in Fig. 2 are unlikely to result from artifacts produced by the pulse protocol. The time-averaged voltage during the 50-ms sequence of pulses (Fig. 2, *inset*) is −98 mV. Thus, whenever the holding potential was near −100 mV, the pulse sequence would not significantly perturb ongoing shifts of slow inactivation. The return to a holding potential of −100 mV was accompanied by slow increases in peak I_{Na}, over the course of minutes, which implies that these relaxations reflect kinetic properties of slow inactivation. The slow relaxations always continued in the same direction as the initial rapid shift in available I_{Na} (for either direction), which shows that these slow components were not caused by nonspecific drifts in peak current. When the holding potential was strongly depolarized, however, the sequence of pulses could conceivably cause a small degree of recovery from slow inactivation. Because the pulse sequence was only 0.3% of the full 15-s sampling interval and the leak pulses were performed after the test pulse, these voltage steps are unlikely to contaminate the measurement of slow inactivation. Simulations with a two-state model showed that any rapid components of slow inactivation (time constants on the order of 2 s or smaller) fully relaxed during the 15-s interval. Conversely, for any slowly recovering component (time constant of ~20 s), the 50-ms pulse sequence was far too brief for any significant degree of recovery. Furthermore, the total number of pulse sequences over 10 min (40) was too small for the development of appreciable pulse-dependent recovery of these very slow components. Thus the relaxations in Fig. 2 reflect kinetic components of slow inactivation. This voltage protocol also demonstrates that the defect in slow inactivation for T698M persists, even on a time scale of minutes. The

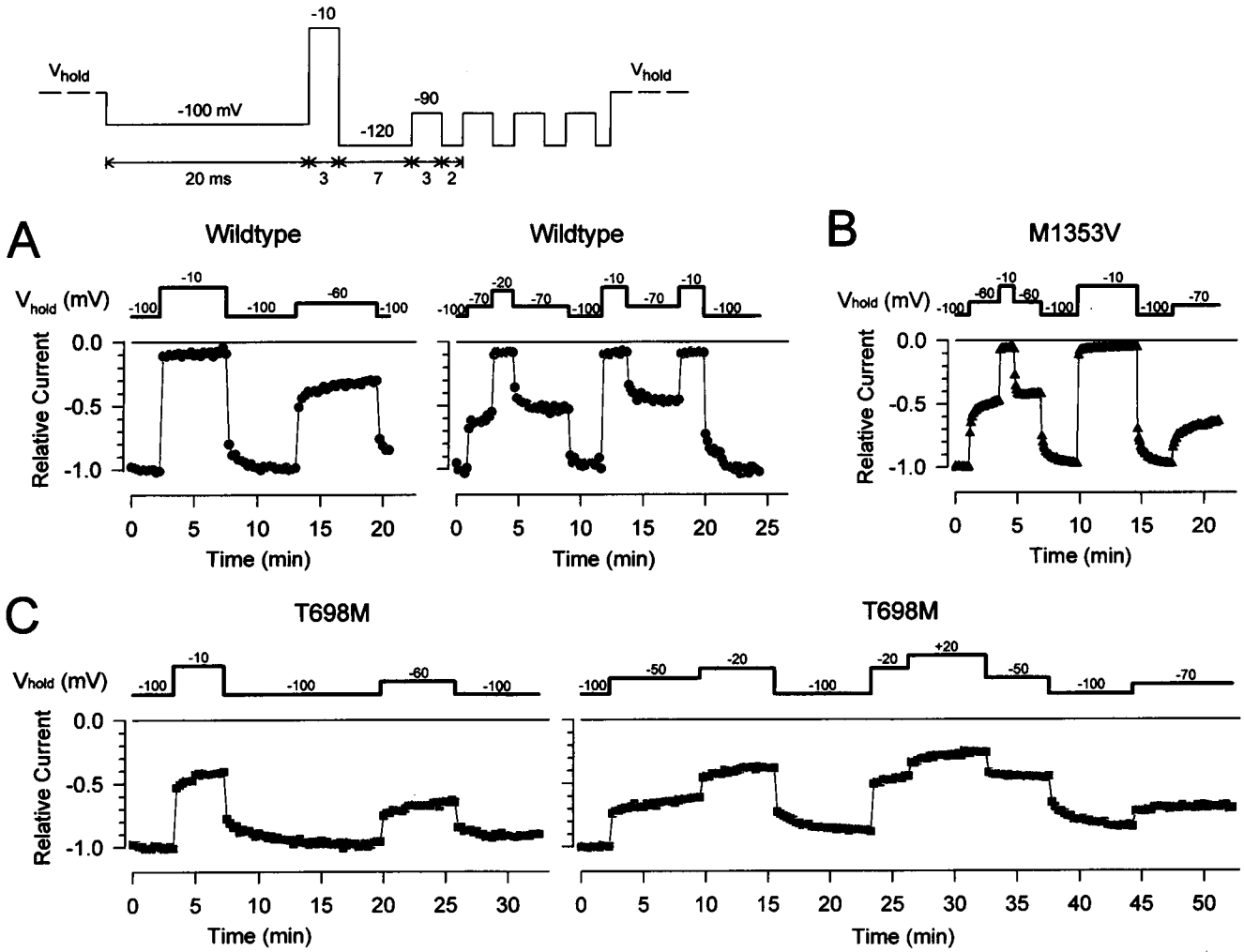

FIGURE 2 Slow inactivation was revealed by long-duration step changes in the holding potential for individual cells. The sequence of voltage steps used to measure slow inactivation is shown by the inset. Each test pulse to −10 mV was preceded by a hyperpolarizing pulse to −100 mV for 20 ms to allow recovery from fast inactivation. A series of four 30-mV depolarizations from −120 mV was performed after the test pulse to measure passive leak currents. Peak Na current was assayed every 15 s, and the holding potential was stepped at intervals ranging from 2 to 12 min. (*A*) At −10 mV, most WT channels were slow inactivated. Less than 10% recovered from inactivation with a 20-ms prepulse to −100 mV. (*B*) One HyperPP mutant, M1353V, exhibited the same extent of slow inactivation as WT channels. (*C*) Another HyperPP mutant, T698M, had disrupted slow inactivation. After holding at −10 mV, about 40% of channels continued to recover within 20 ms. Even stronger depolarization to +20 (*right panel*) for 6 min failed to fully slow inactivate T698M channels. The slow relaxations of peak I_{Na} illustrate that some components of slow inactivation evolved over a time course of minutes.

major limitation of this protocol was the inability to measure the more rapid components of slow inactivation.

A two-pulse protocol was designed to obtain better temporal resolution for the kinetics of slow inactivation (Fig. 3, *inset*). Cells were held at −100 mV, and a conditioning pulse to −10 mV was applied for a preset duration. The conditioning pulse was followed by recovery at −100 mV for a variable interval, from 0.0002 to 10 s. Peak Na current was measured in response to a subsequent test depolarization to −10 mV. Channel availability was measured as the ratio of the peak current during the test depolarization to the current elicited at the onset of the conditioning pulse. Leak currents were assessed by a series of five 5-ms pulses (−120 to −90 mV) 1 s before the conditioning pulse and 1 s after the test pulse. Because WT and mutant channels were not significantly slow inactivated over −120 to −90 mV, the leak pulses were brief, and a 1-s waiting period was used before application of the conditioning pulse, this leakage measurement did not affect our measurements of slow inactivation. Complete recovery between trials was achieved by holding the membrane potential at −100 mV for at least 2–3 times the duration of the conditioning pulse (and a minimum of 1 s for the briefest pulses). A sufficient recovery interval between trials was verified by monitoring the peak I_{Na} elicited by the conditioning pulse. After completion of a series of trials with varying recovery intervals, the duration of the conditioning pulse was incremented (0.01 to 30 s), and the series was repeated.

In Fig. 3 the fraction of available channels from a representative cell expressing WT channels is plotted against the

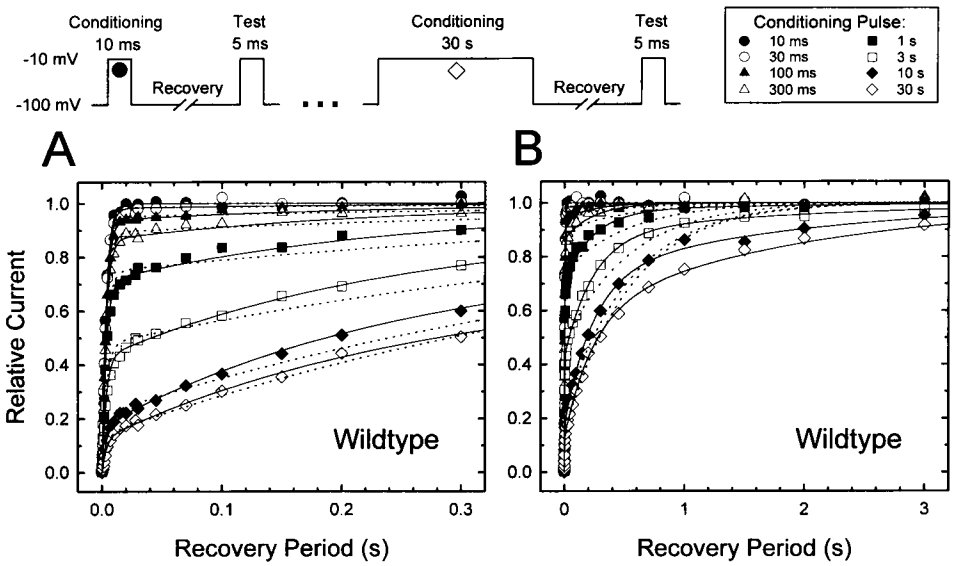

FIGURE 3 Recovery from slow inactivation contained a least two exponential components. A two-pulse protocol (*inset*, described in text) was used to measure recovery from inactivation as the fraction of available I_{Na}. Symbols indicate data sets obtained with a common conditioning pulse duration of 0.01 to 30 s. Data are from one cell expressing WT channels with a peak I_{Na} of 7.1 nA and are plotted on expanded (*A*) and compressed (*B*) time scales to illustrate the multiexponential relaxation more clearly. Curves show χ^2 minimized fits with a fast component and either one (– – –) or two (——) slow components. Fitting of the time constants was constrained to be time-invariant with respect to conditioning pulse duration (see text for details). Fits with a single slow component are inadequate. The dashed curve relaxes too slowly for brief recovery times (*A*) and too quickly at longer recovery intervals (*B*). Parameter values for the fit with a single slow component were τ_{fast} 0.0035 s, τ_{slow} 0.54 s; those of the two slow-component fit were τ_{fast} 0.0034 s, τ_{slow1} 0.24 s, τ_{slow2} 2.0 s.

recovery interval for a series of different conditioning pulse durations. With successively longer conditioning pulse durations, the time course changed from a rapid monoexponential recovery (after 10- or 30-ms conditioning pulses) to a multiexponential recovery with a reduced fast component. The rapid monoexponential component represents the recovery of fast-inactivated channels. The data are shown on expanded (Fig. 3 *A*) and compressed (Fig. 3 *B*) time scales to illustrate that at least two exponential components are required to fit the fraction of channels that recover slowly over several seconds. Solid lines show fits to the data with a fast plus two slow exponential components, and dashed lines are fits using a fast but only a single slow exponential. Each fitted time constant was constrained to be invariant with respect to conditioning pulse duration, which should only influence the initial distribution of channels among various slow- and fast-inactivated states. The relative amplitude of the different components was free to vary with conditioning pulse duration. This constraint was implemented by performing a χ^2 minimized fit with Origin (Microcal) simultaneously over the entire set of data in Fig. 3. The estimated time constant for a single slow component was 0.54 s, and the values for a two-exponential fit were 0.24 and 2.0 s. The inability of a single slow component to approximate the data is demonstrated most clearly by the recovery data after a 3-s conditioning pulse (*open squares*). For short recovery times (<0.3 s) the single slow component grows less rapidly than the data (Fig. 3 *A*), whereas at long recovery times it grows too rapidly (Fig. 3 *B*). If the constraint of an invariant time constant (over different conditioning pulse durations) is relaxed, then individual recovery curves in Fig. 3 can be fitted more closely by individual monoexponential slow components. However, these estimated slow time constants increased fivefold, from 0.15 to 0.8 s, as the conditioning pulse interval increased from 0.3 to 30 s, in violation of any memoryless gating scheme.

When combined, the data in Figs. 2 and 3 indicate that, in addition to fast recovery (a few milliseconds), at least three exponential components were present in the slow phase of recovery from inactivation. Given the limited lifetime of the whole-cell recording mode (even when internal fluoride is used), all of our subsequent pulse protocols focused on the two components of slow recovery shown in Fig. 3 and did not further address the ultraslow component. Nevertheless, the data in Fig. 2 show that the impairment of slow inactivation detected with limited-duration conditioning pulses (30 s to 1 min) persists, even after prolonged depolarizations lasting minutes.

The time course of recovery at −100 mV, after a series of conditioning pulses to −10 mV, is shown for WT and each mutant channel in Fig. 4. The entire range of recovery intervals can be visualized more clearly on this semilogarithmic plot, in which a monoexponential recovery curve has a sigmoidal appearance. Each symbol represents a different conditioning pulse duration, as defined in Fig. 3. For brief conditioning pulse intervals (10, 30, or 100 ms), more than 90% of the current recovered within 20 ms at −100 mV for WT and each mutant, reflecting the rapid monoex-

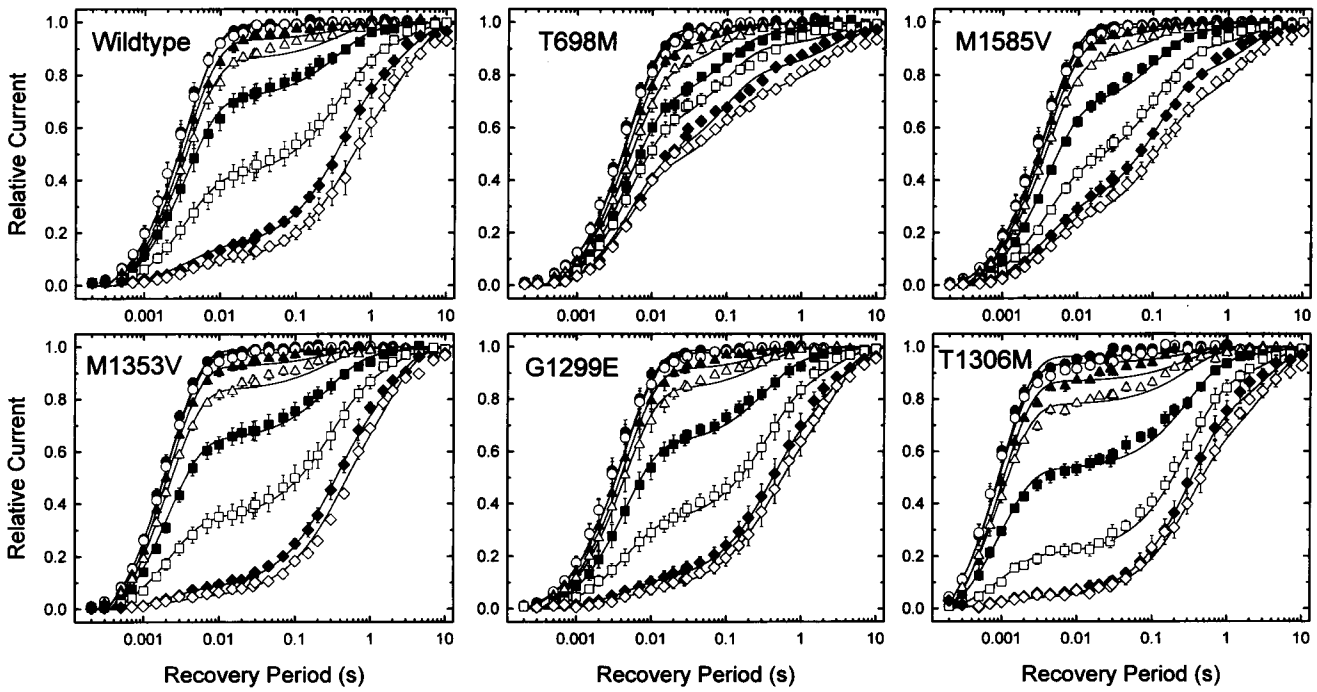

FIGURE 4 Kinetics of recovery from inactivation. The two-pulse protocol shown in Fig. 3 was used to measure recovery from inactivation as the fraction of available I_{Na}. A logarithmic time axis is required to show the range of recovery rates, which varied over nearly 4 orders of magnitude. Symbols indicate the duration of the conditioning pulse, as defined in Fig. 3. For two HyperPP mutants (M1585V and T698M) a large fraction of I_{Na} (30–50%, respectively) recovered within 20 ms, even after the 30-s conditioning pulse. This disruption of slow inactivation is reflected by the smaller shift downward and to the right compared to WT as longer duration conditioning pulses were applied. The T1306M mutant, in contrast, exhibited both accelerated recovery from fast inactivation (seen at short conditioning durations) and enhanced slow inactivation at intermediate conditioning durations (300 ms to 3 s) compared to WT. Symbols show means ± SEM for $n = 7$ (WT, T698M), $n = 6$ (M1585V, T1306M), $n = 5$ (G1299E), or $n = 4$ (M1353V) cells. Smooth curves show the fit obtained by a relaxation function with three exponential components (see Fig. 6).

ponential recovery from fast inactivation. With conditioning pulses of 1 s or longer, slower components of recovery were observed for all channels (*rightward shifted curves* in Fig. 4). However, for two HyperPP mutants, T698M and M1585V, a large fraction of channels (30–50%) recovered within 20 ms at −100 mV, even after a 30-s conditioning pulse.

The sigmoidal components and shifts of the recovery curves in Fig. 4 provide information about the kinetics of both recovery from and entry to inactive states. The overlap of left-shifted curves with brief conditioning pulses (10, 30, 100 ms) demonstrates that at −10 mV no significant entry to slow-inactivated states occurs within 100 ms. Likewise, the approach toward a limiting rightward shift for the longer conditioning pulse durations indicates that at −10 mV the equilibration of channels between the fast- and slow-inactivated states was near steady state by 30 s. The data in Fig. 2 show that prolonged depolarization produced an additional 5–10% change in Na channel availability over several minutes. The kinetic data in Fig. 4 confirm for WT and each mutant that a 20-ms recovery interval at −100 mV provided a clear distinction between the fraction of fast- and slow-inactivated Na channels.

The continuous lines in Fig. 4 show the goodness of fit by the sum of a fast and two slow exponential components. The same time-invariant constraint described for Fig. 3 was used to estimate the time constants for the data in Fig. 4. In addition to providing memoryless estimates for the time constants, this method had the advantage that for each Na channel type there were ample data to define the fastest component (*left-shifted data with short conditioning pulses* in Fig. 4) as well as the slower components (*right-shifted data with long conditioning pulses*). The ability to globally fit the recovery data with a common set of time constants shows that at least three kinetically distinct inactive states were detectable over a time scale of 0.2 to 10,000 ms. The conditioning pulse duration sets the initial distribution among these inactive states, but does not influence the relaxation time constants.

The data recorded after 30-s conditioning pulses in Fig. 4 are superimposed for each mutant and plotted on a linear time scale in Fig. 5. The expanded time scale of Fig. 5 *A* emphasizes the dramatic increase in the fraction of channels that fail to slow-inactivate (i.e., that recover within 20 ms) for T698M and M1585V compared to WT or all other mutants. The compressed time scale in Fig. 5 *B* illustrates that this same data set contained multiple slow exponential components. Thus two HyperPP mutants (T698M and M1585V), but not a third (M1353V), had a marked defect of slow inactivation. Neither myotonia-associated mutation

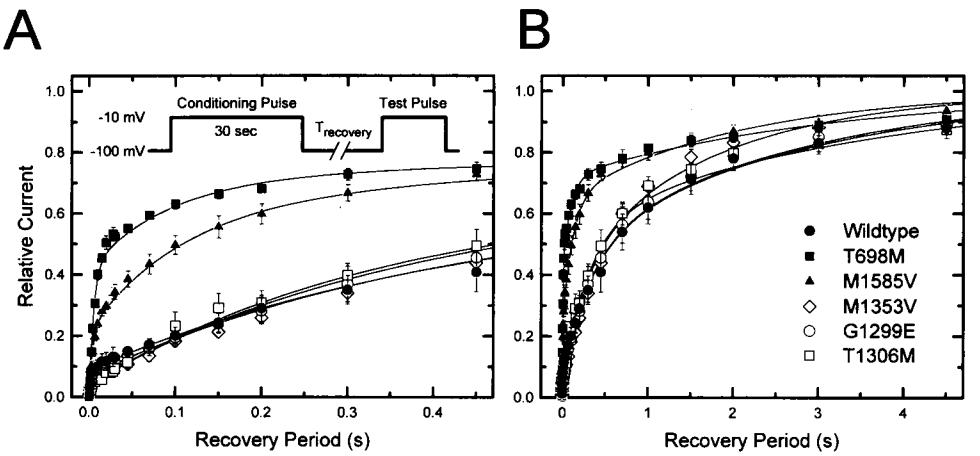

FIGURE 5 Slow inactivation was disrupted for T698M and M1585V mutants. The recovery data recorded after the 30-s conditioning pulse in Fig. 4 are superimposed for each Na channel type. (*A*) An expanded linear time scale shows that 30–50% of channels from M1585V or T698M recover rapidly, with the kinetics of fast inactivation, and hence failed to slow-inactivate within 30 s. (*B*) A compressed linear time scale shows a second component of slow recovery, especially for the T698M mutant.

(G1299E or T1306M) impeded slow inactivation. In fact, the mutant with the most severe defect of fast inactivation (T1306M) showed enhanced slow inactivation (i.e., a smaller fast-recovering component) at intermediate conditioning durations (300 ms to 3 s in Fig. 4) compared to WT.

The time constants of recovery from fast and slow inactivation are shown for each Na channel as a box plot in Fig. 6 *A*. At −100 mV, recovery from fast inactivation (smallest time constant, τ_0) was accelerated for T1306M mutants compared to WT. The slowest component of recovery was comparable for all Na channels tested. For T698M and M1585V, the two mutants with impaired slow inactivation (cf. Fig. 4), the recovery rate for the intermediate component was threefold faster than for WT (Fig. 6 *A*). The relative amplitudes of the three exponential components are shown as a function of conditioning pulse length in Fig. 6 *B*. After brief conditioning pulse durations (<100 ms) to −10 mV, Na channels were in the fast inactivated state (smallest recovery time constant) for WT and all mutants. For the two slow-inactivation defective mutants, T698M and M1585V, a higher proportion of channels remained in the fast-inactivated state, even with long conditioning pulses exceeding 10 s (Fig. 6 *B*, *top panel*). With longer conditioning pulses (0.2–3 s), channels shifted to one slow-inactivated state, S_1. The defining feature of this S_1 state is a recovery time constant of 100–300 ms at −100 mV. After conditioning pulses of 3 s or more, channels populated another slow-inactivated state, S_2, from which recovery at −100 mV occurred with a time constant of 2–3 s. The three exponential components were kinetically well separated, by at least 1–2 orders of magnitude. With progressively longer conditioning pulse durations, Na channels successively populated the fast, S_1, and S_2 inactive states (Fig. 6 *B*), but the connectivity among these states is not uniquely determined by this progression alone.

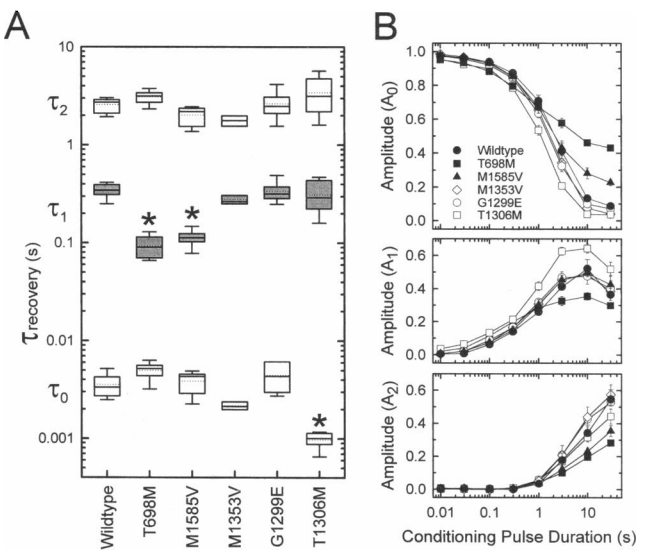

FIGURE 6 Parametric fits to recovery from inactivation at −100 mV. For each cell, the data set for the voltage protocols in Fig. 4 was simultaneously fit to a three-exponential relaxation (one component for fast and two components for slow inactivation) plus a brief delay (~0.3 ms). The time constants were constrained to be shared across the families of curves (different conditioning pulse durations for the same cell), whereas the relative amplitude of each component, for a given conditioning duration, was free to vary independently. (*A*) Three distinct time constants were well separated by 1–2 orders of magnitude for each channel type. The box plot shows the mean (*dotted line*), median (*solid line*), 75% confidence interval (*box*), and 95% confidence interval (*bar*). Asterisks indicate differences from WT at p values < 0.001 (t-test). Recovery from fast inactivation, τ_0, is hastened for the T1306M mutant. For the two HyperPP mutants with disrupted slow inactivation, T698M and M1585V, recovery of the intermediate component was accelerated about threefold. The slowest component of recovery at −100 mV was not greatly altered by any of the mutants. (*B*) The relative amplitudes for the fast (A_0), intermediate (A_1), and slow (A_2) components are plotted against conditioning pulse duration. All Na channels shifted toward the slower recovery components as the conditioning time increased. The fastest recovery component, A_0, was persistently high at long conditioning durations for T698M and M1585V, because slow inactivation was less complete for these two mutants. Symbols show means ± SEM; n is listed in Fig. 4.

Voltage dependence of slow inactivation

The voltage dependence of entry to and recovery from slow inactivation was determined by varying the potential of the

conditioning or recovery pulses, respectively. The kinetics of entry to slow inactivation at different membrane potentials are shown in Fig. 7. Fig. 7 *A* shows the relative current elicited by conditioning pulses for varying durations in cells transfected with WT or T698M rSkM1. The entry rate and extent of slow inactivation increased with more depolarized conditioning pulses for both channel types. For the T698M mutant, however, the fraction of channels that entered the slow inactivated state(s) within 60 s was reduced, as demonstrated by the larger plateau currents in Fig. 7 *A*.

A double-exponential relaxation function (plus a nonzero steady-state value) was required to fit the decay in relative

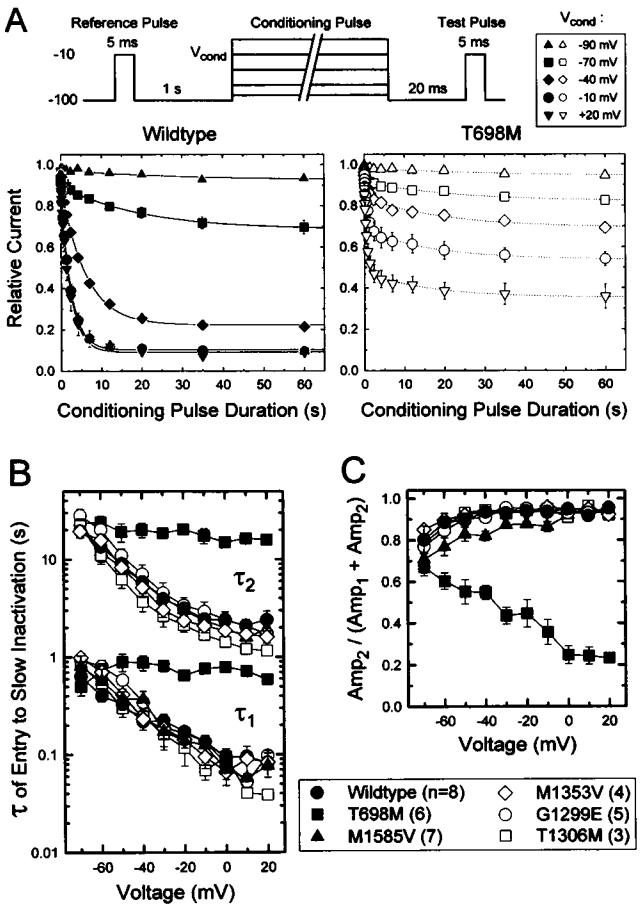

FIGURE 7 Voltage dependence for the onset of slow inactivation. (*A*) Entry to slow inactivation was measured as the peak I_{Na} elicited at −10 mV, after a conditioning pulse of variable duration. Current amplitudes were normalized to the reference peak I_{Na} elicited from a holding potential of −100 mV. The conditioning and test pulses were separated by a 20-ms hyperpolarization to −100 mV to allow recovery from fast inactivation (see schematic of voltage protocol). Symbols denote different conditioning voltages, and the smooth curves show χ^2 minimized fits of a double exponential relaxation plus a constant. The larger steady-state currents for T698M show that slow inactivation was less complete for this mutant compared to WT. Entry to slow inactivation was faster at depolarized potentials for all channels. The time constant of each component (*B*) and relative amplitude of the slow component (*C*) are shown as a function of conditioning pulse potential. Parameters were averaged from best fits to individual cells, and error bars show ± SEM; *n* for *A* and *B* is listed after each mutation.

I_{Na} over the full range of conditioning pulses, 0.01–60 s. The voltage dependence of the time constants and the relative amplitude of the slower component are shown in Fig. 7, *B* and *C*. Similar to the kinetics of recovery (cf. Fig. 6), the two components of entry to slow inactivation were well separated, by about 20-fold. Except for T698M, entry to slow inactivation was dominated (~90%, Fig. 7 *C*) by the slow component that decayed on the order of seconds. Over −70 to −30 mV, the slow time constant was reduced an *e*-fold per ~25 mV for WT and the other four mutant channels (Fig. 7 *B*). For T698M channels, the amplitudes of the fast and slow components were more comparable. Furthermore, the unconstrained fits across different conditioning potentials yielded voltage-independent time constants (Fig. 7 *B*), and a shift in the relative amplitude from the slow toward the fast component with larger depolarization (Fig. 7 *C*). The χ^2 error and appearance of the fit were noticeably degraded if the relative amplitude of the slow component was constrained to be 0.9 to match the behavior of the other Na channel types. It is noteworthy that a voltage-independent time constant was not a required consequence of disrupted slow inactivation. The M1585V mutant, which also had impaired slow inactivation (cf. Figs. 4 and 5), had voltage-dependent time constants indistinguishable from WT channels. Furthermore, like the other Na channels tested, T698M enters slow inactivation faster and more completely at depolarized potentials, albeit to a lesser extent.

Data from the entry to slow inactivation protocol also enabled us to define the voltage dependence of steady-steady slow inactivation, $s_\infty(V)$. As shown for WT and T698M channels in Fig. 7 *A*, the reduction in relative I_{Na} approached a constant value within 60 s. The other four Na channel mutants entered slow inactivated state(s) at rates similar to those of WT channels (Fig. 7 *B*) and plateaued at 60 s (data not shown). Although relaxations over durations longer than 60 s were present, as shown in Fig. 2, the amplitude of these components was small in comparison to the data in Fig. 7. The steady-state inactivation parameter, s_∞, was thus defined as the fraction of channels that recovered within 20 ms at −100 mV, after a 60-s conditioning pulse. s_∞ therefore represents the fraction of channels not slow inactivated, analogous to h_∞, the fraction of channels not fast inactivated. The voltage dependence of s_∞ is shown for WT and each of the mutants in Fig. 8. The HyperPP mutants, T698M and M1585V, showed the greatest changes in s_∞. The voltage dependence of slow inactivation was less steep, shifted toward the right (depolarized), and incomplete. For these two mutants, the increased fraction of current that failed to slow-inactivate persisted, even with progressively larger depolarizations. The data in Fig. 8 were fit by a single Boltzmann plus a constant term; the parameter values are listed in Table 1. For WT channels, the midpoint voltage of the $s_\infty(V)$ curve occurred at potentials depolarized by 5 mV relative to that of fast inactivation, $h_\infty(V)$, −62 compared to −67 mV, respectively.

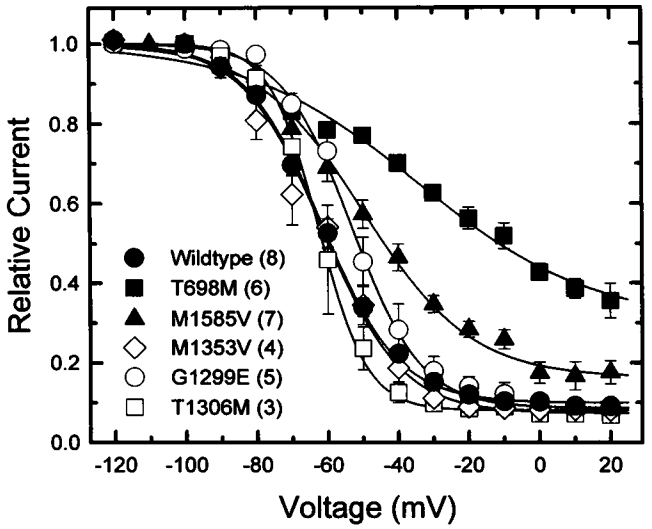

FIGURE 8 Steady-state voltage dependence of slow inactivation. Peak I_{Na}, measured after a 60-s conditioning pulse, was normalized by the peak current elicited from a holding potential of −100 mV. Test and control currents were measured at −10 mV. The conditioning and test pulses were separated by a 20-ms hyperpolarization to −100 mV to allow channels to recover from fast inactivation. Smooth curves show χ^2 minimized fits of the data by a Boltzmann function plus a constant term (parameter values listed in Table 1). Symbols show mean values ± SEM; n is listed after each mutation.

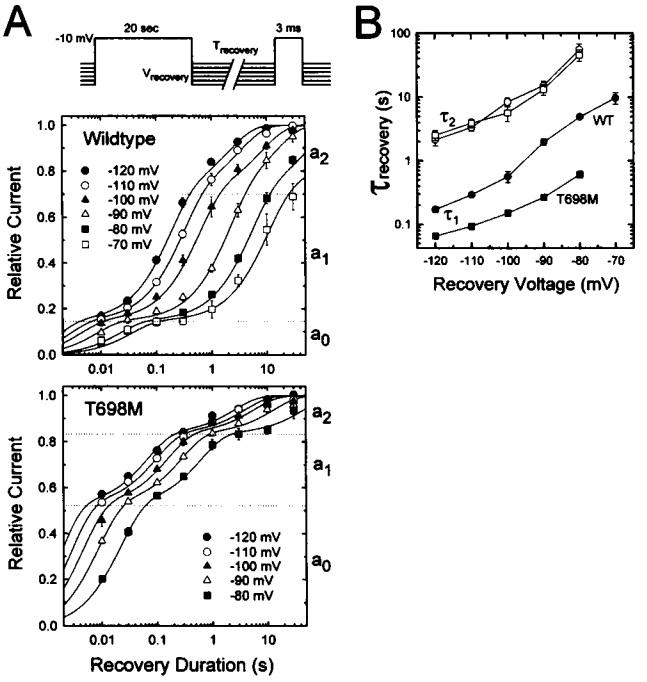

FIGURE 9 Voltage dependence of recovery from slow inactivation. (*A*) Relative current from WT and T698M channels as a function of recovery duration is plotted on a logarithmic time axis. Inset shows the voltage protocol. Data are mean values from five (WT) or six (T698M) cells. Smooth curves show χ^2 minimized fits with a triple exponential relaxation. The time constant of the fastest component of recovery, $\tau_0(v)$ (not shown), was assumed to follow kinetics of recovery from fast inactivation (cf. Fig. 4). The relative amplitudes of the three components are indicated by horizontal dotted lines (fastest to slowest): 0.14, 0.56, 0.30 for WT and 0.52, 0.31, 0.17 for T698M. (*B*) Both time constants of recovery from slow inactivation, τ_1 and τ_2, became longer at more depolarized potentials for both WT and T698M. Whereas τ_2 was unaffected by the mutation over −120 to −80 mV, τ_1 was three- to fivefold faster for T698M compared to WT.

The voltage dependence of recovery from slow inactivation was measured for WT and T698M channels over a range of −80 to −120 mV. The voltage protocol is illustrated in the inset of Fig. 9. With this protocol, the control I_{Na} (elicited by application of the conditioning pulse) and test I_{Na} were elicited from the same starting potential. Slow inactivation was induced by a 20-s conditioning pulse to −10 mV. The time course of recovery from slow inactivation is shown at several voltages plotted on a logarithmic time axis in Fig. 9 *A*. The smooth curves were generated with mean parameter values from fitting each cell to a three-exponential relaxation (one component for fast inactivation recovery and two components for slow recovery). Because all of the recovery data were measured from the same initial condition (−10 mV for 20 s), the relative amplitudes of the three components were the same for data at all recovery potentials. The mean amplitudes (a_0, a_1, a_2) are indicated in Fig. 9 *A* by the dotted horizontal lines. About one-half ($a_0 \approx 0.52$) of T698M channels recover with a fast time constant, τ_o, equal to the time constant for recovery from fast inactivation. This component reflects the large fraction of T698M channels that fail to slow inactivate. The time constants for the slower two components (τ_1 and τ_2), which reflect recovery from slow inactivated state(s), are shown as a function of recovery potential in Fig. 9 *B*. The voltage dependence of these time constants was similar, ~20 mV/*e*-fold between −120 and −100 mV, for the fast and slow components and for both WT and T698M channels. However, the faster recovery time constant, τ_1, was about threefold faster for T698M than WT between −120 and −100 mV, which is consistent with a destabilized slow inactive state for the mutant. Interestingly, the T698M mutation did not affect either the slower recovery time constant, τ_2, or the relative distribution of channels among the two slow-inactivated states, $(a_1/(a_1 + a_2) \approx 0.65$, for both WT and T698M).

Slow inactivation reduced late Na currents and produced use-dependent block

The disruption of slow inactivation for a subset of HyperPP mutants (T698M and M1585V) should produce measurable differences in late Na currents and use-dependent block. One form of inactivation defect for mutant Na channels has previously been characterized as the persistent current at 50 ms, relative to the peak I_{Na} (Cannon et al., 1993; Hayward et al., 1996). Slow inactivation may attenuate this persistent current and thereby reduce the consequence of this anomaly. We sought to directly measure the influence of slow inactivation on the persistent current by recording I_{Na} during a 6.5-s depolarization. A split time base was used to sample

the initial transient at 50 kHz (0–30 ms), and the remaining 6.47 s was sampled at 200 Hz. The T1306M mutant has a large persistent current (Hayward et al., 1996), so the initial peak and any decay of the persistent current can be visualized on the same amplitude scale. Fig. 10 *A* shows that the persistent I_{Na} at 30 ms decayed appreciably over several seconds. Slow inactivation was approximately 90% complete at −10 mV for T1306M (Fig. 8), so the decline in the I_{Na} after 30 ms could be due to slow inactivation. If decay of the persistent I_{Na} is due to slow inactivation, then the decline should be reduced for mutants with defective slow inactivation. Current traces for WT and each mutant were normalized to the amplitude at 30 ms and are superimposed in Fig. 10 *B*. For WT, M1353V, and T1306M channels (all with intact slow inactivation), the persistent current decayed by 90% within 6.5 s. Two HyperPP mutants, T698M and M1585V, have disrupted slow inactivation, and the persistent currents decayed by only 35% and 80%, respectively, to a plateau on this time scale. The degree of attenuation observed for each channel type was comparable to that predicted from the steady-state slow inactivation relation (Fig. 8). Thus slow inactivation most likely attenuated the persistent I_{Na}, measured after tens of milliseconds. For all channel types in Fig. 10, the decay rate after the initial 30 ms was faster than the rate of entry to slow inactivation (Fig. 7). We attribute this accelerated relaxation to contributions from fast inactivation that remain appreciable on this expanded amplitude scale, even at long times compared to τ_h.

In theory, slow inactivation could also contribute to cumulative trapping of Na channels in an inactive state during repetitive discharges. This form of use-dependent block could limit the duration of the trains of repetitive discharges that occur in myotonia. To simulate myotonia, 5-ms depolarizations to −10 mV were applied at a frequency of 50 Hz from a holding potential of −80 mV. Neither P/N leak pulses nor brief hyperpolarizing recovery steps were used in the pulse train. The amplitude of the peak I_{Na} measured during each 5-ms pulse was normalized and plotted as a function of pulse train duration in Fig. 11, which shows every 20th pulse. Fast inactivation caused a 50% reduction in available I_{Na} within the first 20 pulses for both WT and T698M channels (Fig. 11, *inset*). A slower component of use-dependent block developed in WT but not T698M channels. Relative to the available current after fast use-dependent block, slow inactivation produced an additional 42% block in WT channels, whereas only about 10% occurred in T698M channels (Fig. 11).

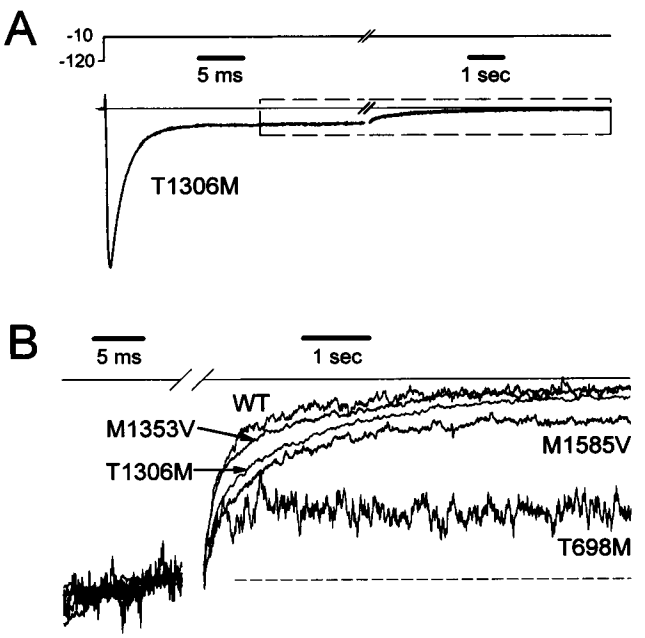

FIGURE 10 Persistent I_{Na} currents were attenuated by slow inactivation. (*A*) Sodium current conducted by a T1306M channel is shown on a split time scale. The persistent Na current at 30 ms decayed substantially over a period of seconds. (*B*) Current recordings from WT and four mutant channels were normalized to the amplitude of the persistent I_{Na} at 30 ms and superimposed. Further decay of I_{Na} over 6.5 s was comparable to that predicted from s_∞ (−10 mV) in Fig. 8. Tracings in *B* were filtered digitally (SigmaPlot) with cutoff frequencies of 1 kHz and 4 Hz for the fast and slow time bases, respectively. The persistent I_{Na} (nA) at 30 ms for these cells was 0.12 for WT, 0.024 for T698M, 0.12 for M1585V, 0.20 for M1353V, and 0.26 for T1306M. The ratio of persistent to peak I_{Na} for other cells in this study was (mean % ± SD, *n*): 0.29 ± 0.07, 8 for WT; 0.79 ± 0.19, 8 for T698M; 0.88 ± 0.25, 7 for M1585V; 0.42 ± 0.09, 5 for M1353V; 0.43 ± 0.08, 5 for G1299E; 8.5 ± 2.4, 5 for T1306M.

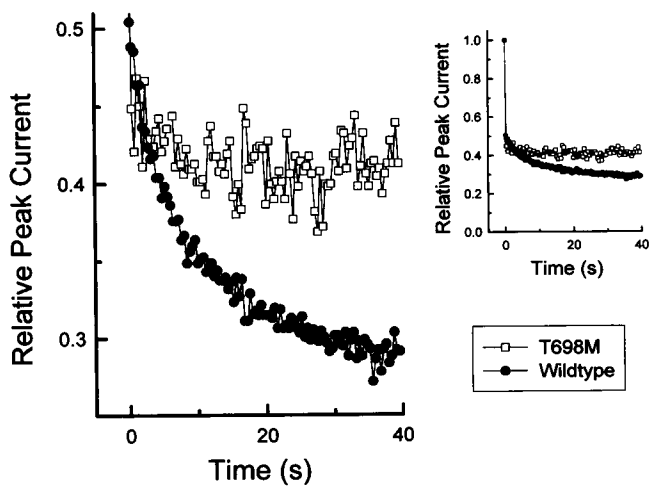

FIGURE 11 Use-dependent reduction of I_{Na} from slow inactivation is greater for WT than T698M channels. Sodium currents were elicited by depolarization to −10 mV from a holding potential of −80 mV. The 5-ms depolarization was applied at a rate of 50 Hz, and the relative peak I_{Na} is plotted for every 20th stimulation for representative WT (●) and T698M (□) cells. No hyperpolarized prepulses or small depolarizations to measure leakage currents were applied. The inset shows that fast inactivation produced a 50% use-dependent reduction in peak I_{Na} within the first 20 pulses (rapid drop between the first and second data points) for both WT and T698M channels. Over tens of seconds, an additional use-dependent block developed for WT channels but was minimal for T698M.

DISCUSSION

Slow inactivation of heterologously expressed Na channels was characterized for WT and five mutants associated with periodic paralysis or myotonia. The primary finding was that two HyperPP mutations, T698M and M1585V, disrupt slow inactivation. For these two mutants, steady-state slow inactivation was less complete, was shifted toward depolarized potentials, and was less voltage dependent. Destabilization of slow inactivation arose primarily from an increased rate of recovery rather than slowed entry. Cummins and Sigworth (1996) found a similar disruption of slow inactivation when T698M (without cotransfection of the β_1 subunit) was expressed in HEK cells. A defect in slow inactivation likely contributes to episodes of paralysis (see below) but is not required. The T698M and M1585V mutations combined account for over 90% of all genotyped kindreds with HyperPP, but there are at least three other mutations in SkM1 in which the presenting symptom is episodic weakness. The M1353V mutation causes a HyperPP phenotype (Lehmann-Horn et al., 1993), and yet our data show this mutant has preserved slow inactivation. Neither of the other two mutants we tested had defects of slow inactivation. The T1306M mutation causes PMC, which presents with muscle stiffness aggravated by movement or cold. Even though slow inactivation is intact for T1306M channels, patients with this mutation become weak with severe muscle cooling (Ptacek et al., 1993). The G1299E mutation causes pronounced myotonia, in the absence of a defect in slow inactivation.

Multiple exponential components were observed in the recovery from and entry to slow inactivation. Cummins and Sigworth (1996) reported that two or even three exponentials were required to obtain good fits to slow recovery of rSkM1 expressed in HEK cells. When human SkM1 was studied in oocytes, however, Featherstone et al. (1996) found that a single exponential relaxation provided adequate fits to both recovery from and entry to slow inactivation, as measured over a time scale of 60 s. Although arguments can be made when comparing single to two exponential fits with regard to improved goodness of fit versus redundant parameters, the Markov constraint of time-invariant transition rates provided additional evidence for the existence of multiple components of slow inactivation in our data. After a specific conditioning pulse interval, recovery of the slow inactivated component was often approximated fairly well by a single exponential. Across different (long) conditioning pulse intervals, however, independent single-exponential fits yielded recovery time constants that changed fivefold with conditioning pulse duration. Global fitting of a cell's entire set of recovery data simultaneously showed that two time-invariant exponential components, whose relative amplitude varied with conditioning pulse duration, produce a good fit (cf. Fig. 4) without violation of the assumptions of memoryless gating transitions. We propose that both of the components defined by our χ^2 fits should be regarded as features of slow inactivation. Specifically, the multiexponential relaxation we detected is not due to the anomalous "slow mode" of fast inactivation for two reasons. First, the kinetics of entry are not comparable. The slow mode of fast inactivation is detectable in HEK cells as an additional slowly decaying phase of I_{Na} elicited by a step depolarization (Ukomadu et al., 1992). Entry to the slow mode at -10 mV has a time constant of 8 ms, whereas the faster of our two components for entry to slow inactivation at -10 mV has a time constant of 100 ms (Fig. 7 *B*). Second, the magnitude of the slow mode in HEK cells (<5% of total I_{Na}) is not consistent with the large relative amplitudes observed for the two components during recovery from slow inactivation (40 to 60%, cf. Fig. 6 *B*).

Heterologous expression of mutant Na channels has provided some insight into functional domains important for slow inactivation. Rudy (1978) showed that slow inactivation remains intact after the removal of fast inactivation by internal treatment with protease. Consistent with this observation, mutations in the cytoplasmic linker between domains III and IV do not impede slow inactivation. The IFM→QQQ mutation (1303–1305 in rSkM1) profoundly disrupts fast inactivation (West et al., 1992), and yet neither this mutation (Featherstone et al., 1996) nor F1304Q (Cummins and Sigworth, 1996) impairs slow inactivation. Two III–IV linker mutations in our study, G1299E and T1306M, disrupted fast inactivation, but neither mutant impeded slow inactivation. In fact, the mutant with the most severe defect of rapid inactivation, T1306M, had a faster rate of entry to slow inactivation compared to WT (Figs. 4 and 6 *B*), consistent with previous interpretations of competition between these two processes (Rudy, 1978; Valenzuela and Bennett, 1994; Featherstone et al., 1996). The two mutations that did impede slow inactivation, T698M and M1385V, are both predicted to lie near the cytoplasmic ends of transmembrane segments II-S5 and IV-S6, respectively. These residues may be part of the inner vestibule of the pore, because mutations here disrupt fast inactivation, possibly due to impaired docking of the III–IV linker. The slow-inactivation defects produced by mutations at these residues suggest that a structural rearrangement of the cytoplasmic mouth of the pore occurs with slow inactivation. The outer mouth of the pore (W402 in the P region of domain I in rSkM1) is critical for the anomalously slowed inactivation of SkM1 in the oocyte expression system (Balser et al., 1996). This form of inactivation in oocytes, however, may be the equivalent of the "slow mode" of fast inactivation observed in HEK cells and is probably not slow inactivation as measured in the present study.

Data from heterologous expression studies must be interpreted with caution because slow-inactivation properties are different for endogenous Na channels in skeletal muscle. Loose patch recordings from amphibian (Almers et al., 1983) and mammalian (Ruff et al., 1987) skeletal muscle showed that the voltage dependence of steady-state slow inactivation was shifted by -20 mV (hyperpolarized) relative to steady-state fast inactivation. The midpoint of the

$s_\infty(V)$ curve was equal to or slightly depolarized (5–7 mV) relative to the $h_\infty(V)$ relation for heterologously expressed rSkM1 in HEK cells without β_1 (Cummins and Sigworth, 1996), HEK cells with β_1 (present study), or oocytes with β_1 (Featherstone et al., 1996). One possible explanation for the discrepancy is that 20-ms conditioning pulses were used to measure $h_\infty(V)$ in the loose patch studies. Such a brief conditioning pulse may have caused an apparent rightward shift of $h_\infty(V)$ (cf. Fig. 1). The midpoint of $h_\infty(V)$ was -70 to -77 mV in the loose patch experiments (Ruff et al., 1987), whereas other studies have reported values from -80 to -100 mV.

Functional consequences of combined fast and slow inactivation defects

A tailored, two-pulse voltage protocol with constraints on the conditioning and recovery (hyperpolarized) pulse durations is required to measure slow inactivation of Na channels. Such constraints raise the question of how slow inactivation influences the excitability of muscle under physiological conditions. Fig. 11 shows experimental evidence that slow inactivation may reduce Na channel availability during a prolonged high-frequency train of discharges, such as occurs in myotonia. In addition, the I_{Na} that persists for tens of milliseconds in depolarized mutant channels decays over seconds because of slow inactivation (Fig. 10). Thus slow inactivation could attenuate I_{Na} during depolarization-induced attacks of paralysis in which the resting potential is -60 to -45 mV. We have explored the influence of slow inactivation on excitability by incorporating a slow inactivation gating parameter into our muscle cell model (Cannon et al., 1993).

The model consisted of two membrane compartments, separated by an access resistance, to simulate sarcolemma and T-tubules. Each membrane compartment contained sodium, potassium (delayed rectifier), and leak conductances. The open channel I-V was ohmic, and open probability was computed using the Hodgkin-Huxley equations (Cannon et al., 1993). Potassium accumulation in the T-tubule space was computed from the balance between I_K across the T-tubule membrane and passive diffusion with the extracellular $[K^+]$. Model parameters were identical to those in our original simulations (Cannon et al., 1993), except that fast inactivation kinetics for Na channels were altered to mimic responses of heterologously expressed rSkM1, as described by Hayward et al. (1996). Slow inactivation was incorporated by multiplying the Hodgkin-Huxley open probability term, m^3h, by a slow inactivation term, $s(V, t)$. In using this multiplicative approximation, we do not mean to imply mechanistic independence of activation, fast inactivation, and slow inactivation. Activation and fast inactivation are coupled (Aldrich and Stevens, 1987), and slow inactivation may be coupled to activation (Rudy, 1978).

Steady-state behavior

The steady-state behavior of the model was simulated to define the conditions under which additional equilibrium potentials occurred. These depolarized equilibria correspond to states of paralysis for the muscle. The steady-state voltage dependence of slow inactivation, $s_\infty(V)$, was modeled by the Boltzmann fits shown in Fig. 8. The functional consequences of slow inactivation were studied in the context of previously identified defects of fast gating in mutant Na channels (Cannon and Strittmatter, 1993; Cummins et al., 1993). Two fast-gating defects were studied independently. A persistent Na current, 1–10% of the initial peak (5- to 50-fold greater than WT) has been observed for many mutations associated with paralytic phenotypes. This defect was introduced to the model as a fraction, f, of I_{Na} that failed to fast inactivate by replacing h with $(1 - f)h + f$. The other simulated fast-gating defect, a hyperpolarized shift in the voltage dependence of activation as measured by relative peak conductance $G(V)$, is at maximum for T698M and is particularly relevant to slow inactivation, because this mutant had the greatest alteration in $s_\infty(V)$. A shift in $G(V)$ was achieved by replacing $\bar{V}_m$ in the forward and backward rate constants for m by $\bar{V}_m + \delta V$.

Fig. 12 *A* shows equilibrium potentials for the model as the fraction of fast inactivation failure was increased from 0 to 0.1 when there was no slow inactivation ($s_\infty(V) = 1$), WT slow inactivation, or T698M-like slow inactivation. The normal resting potential of -85 mV remained a possible equilibrium voltage, over the entire range of f, for each type of slow inactivation. New depolarized equilibrium potentials occurred as f increased. Of the three equilibria at a given f, -85 mV was always stable, the intermediate one was always unstable, and the most depolarized represented a possible paralytic state. Thus, for large f, the system often had two simultaneous stable equilibrium potentials. As expected from the multiplicative relation between fast and slow inactivation variables in the model, a larger degree of fast inactivation failure, f, was required to produce paralysis as slow inactivation was varied from none to T698M to WT. Because $s_\infty(V)$ does not decline to 0 even for WT channels (Fig. 8), a large enough fast-inactivation defect can produce sustained paralysis (a stable depolarized equilibrium potential), even in the absence of a slow inactivation defect. On the other hand, a disruption of slow inactivation, as seen in T698M, increased the susceptibility to paralysis, because stable depolarized equilibria occurred with a smaller fast inactivation defect, f.

The effect of shifting the voltage dependence of Na channel activation on equilibrium states of the model is shown in Fig. 12 *B*. With large enough shifts in $G(V)$, the only stable equilibrium potential was depolarized relative to the normal resting potential of -85 mV. As slow inactivation increased, a greater shift in $G(V)$ was required to produce paralysis. Comparison of Fig. 12, *A* and *B*, however, shows that slow inactivation more effectively compensates for incomplete fast inactivation than for shifts in

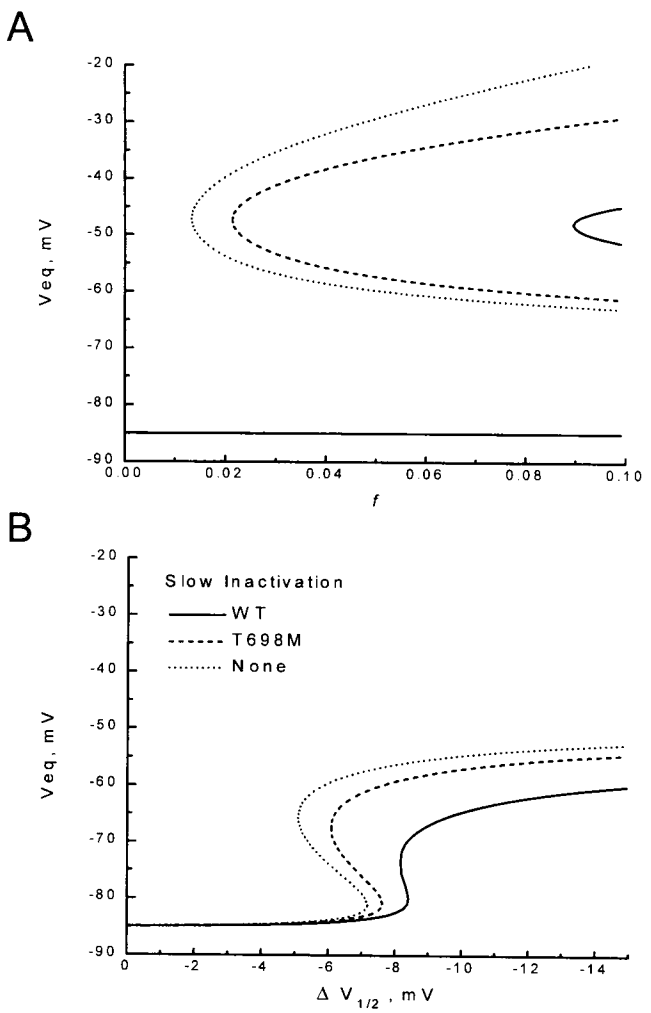

FIGURE 12 Slow inactivation attenuates the consequences of fast gating defects. Equilibrium solutions were computed for a simulated muscle cell (*A*) as the fraction of I_{Na} that failed to fast inactivate, f, was increased or (*B*) as the voltage dependence of Na channel activation was shifted in the hyperpolarizing direction. Simulations were computed with WT (——), T698M (– – –), or no (·····) slow inactivation. The equilibrium potential at −85 mV in *A* occurred for all values of f for all three types of slow inactivation (lines are superimposed).

$G(V)$. This difference occurred because of the range of voltages over which the fast gating defects altered Na channel availability. A hyperpolarized shift of $G(V)$ produced an increased window current or region of overlap between $h_\infty(V)$ and $m_\infty(V)^3$. However, this anomalous steady-state current occurred over only a limited voltage range (−80 to −50 mV) in which $s_\infty(V)$ remained high, even for WT channels, in which case slow inactivation could not prevent paralysis. By contrast, incomplete fast inactivation produced an anomalous steady-state current at all voltages greater than −60 mV, where Na channels began to open. This persistent Na current created depolarized stable equilibria in the −45 to −20 mV range, where slow inactivation of WT channels was much more complete than for T698M mutants (Fig. 8). Thus slow inactivation had a more pronounced effect on preventing paralysis from incomplete fast inactivation than from a depolarized shift in activation.

Dynamic behavior

The simulated behavior of muscle in response to current injection or shifts in extracellular $[K^+]$ shows how differences in slow inactivation of Na channels affect trains of myotonic discharges or the stability of depolarized equilibrium potentials. Before such a computation can be performed, however, a quantitative description of the voltage and time dependence of slow inactivation is required. The kinetic behavior of slow inactivation was complex, with multiple exponential components (Figs. 2–7, 9). In the model simulation, slow inactivation was approximated by a voltage-dependent, single-exponential relaxation to the steady-state value. Data for entry to and recovery from slow inactivation, such as those in Figs. 7 and 9, respectively, were fit to a single exponential. The voltage dependence of the time constants obtained from these fits is shown in Fig. 13. This single-exponential approximation was more accurate for entry than recovery, as expected from the relative amplitudes of the components from the double-exponential fits in Figs. 7 and 9. Over the physiological voltage range of −100 to 20 mV, the time constant for slow inactivation, τ_s, varied between 0.5 and 8 s. A set of voltage-dependent forward and backward transition rates, $\alpha_s(V)$ and $\beta_s(V)$,

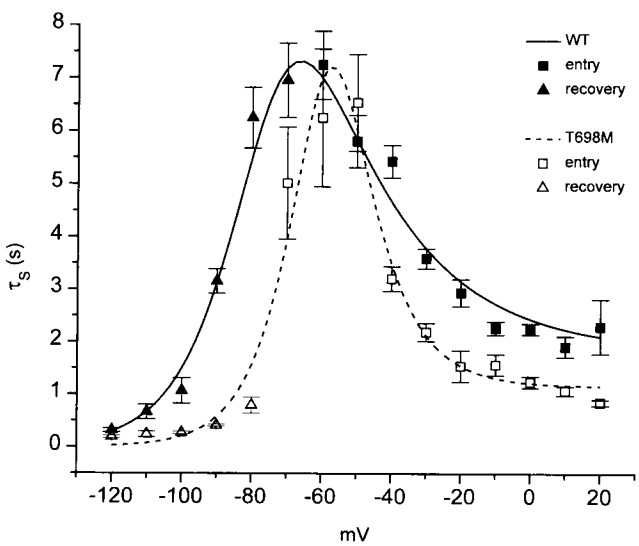

FIGURE 13 Voltage dependence for a single-exponential approximation of slow inactivation. For WT and T698M channels, the data for entry to (Fig. 7) and recovery from (Fig. 9) slow inactivation were fit by a single exponential plus a constant. Time constants are plotted as a function of membrane potential during the conditioning pulse (entry data, □, ■) or recovery interval (recovery data, △, ▲). Curves show the best fit for a two-state model with voltage-dependent forward (β_s) and backward (α_s) rates from non-slow-inactivated to slow-inactivated, where $\beta_s(V) = \bar{\beta}_s/[1 + \exp(-(V - V_s)/k_{\beta s})]$ and $\alpha_s(V) = \bar{\alpha}_s\exp(-V/k_{\alpha s})$. Parameter values for WT channels were $\bar{\alpha}_s = 1.6 \times 10^{-4}\ s^{-1}$, $k_{\alpha s} = 12$ mV, $\bar{\beta}_s = 0.5\ s^{-1}$, $k_{\beta s} = 23$ mV, $V_s = -32$ mV; and for T698M channels, $\bar{\alpha}_s = 1.9 \times 10^{-4}\ s^{-1}$, $k_{\alpha s} = 9.8$ mV, $\bar{\beta}_s = 0.78\ s^{-1}$, $k_{\beta s} = 11$ mV, $V_s = -32$ mV.

similar to $\alpha_h(V)$ and $\beta_h(V)$ for fast inactivation, was used to empirically fit $\tau_s(V) = 1/[\alpha_s(V) + \beta_s(V)]$, as shown in Fig. 13. The voltage dependence of steady-state slow inactivation, $s_\infty(V)$, was described by a Boltzmann function plus a constant term, as listed in Fig. 8. For the simulation, the slow inactivation parameter, $s(V, t)$, was defined by $ds/dt = (s_\infty - s)/\tau_s$.

The consequence of the slow inactivation defect for T698M channels on the excitability of a simulated cell is shown in Fig. 14. Because the HyperPP phenotype is dominantly expressed, two types of Na current were used for the simulation. Fifty percent of the simulated current was modeled with WT parameters, and the other half was modeled with T698M parameters. The T698M parameters included defects in fast gating (−7 mV shift in activation; fractional failure of fast inactivation, $f = 0.02$) as well as the disruption of slow inactivation shown in Figs. 8 and 13. For simulated heterozygous muscle, a suprathreshold stimulus applied for 100 ms elicited a train of discharges (Fig. 14 *A*). The myotonic discharges persisted for the entire 5-s simulation, after which the membrane potential was reset to the normal rest value of −85 mV. Elevation of extracellular $[K^+]$ from 4 to 5.5 mM caused a spontaneous depolarization, followed by a brief myotonic run that terminated in a stable depolarization at −46 mV. The persistent Na current (proportional to $m_\infty^3 f s_\infty$, because $h_\infty(V) \approx 0$) produced the large depolarized shift in V_{rest}, beyond the shift in the Nernst potential for potassium, E_K. The model was refractory from this depolarized state. Subsequent current injection failed to elicit action potentials, similar to the behavior of HyperPP muscle during attacks of weakness. Fig. 14 *B* shows that the slow inactivation defect for T698M channels contributed to the generation of myotonia and paralysis. The slow inactivation parameters for the T698M channels were changed to WT values, whereas the defects in activation and fast inactivation were retained. In 4 mM $[K^+]_o$, the current stimulus elicited repetitive discharges, but the firing did not persist beyond the duration of the stimulus. Stepping $[K^+]_o$ from 4 to 5.5 mM caused a rapid small depolarization (shift in E_K for the surface membrane) followed by a slower, mild depolarization as extracellular K equilibrated with the T-tubule space. From the new resting potential of −75 mV, the same current stimulus now elicited a train of discharges that persisted for about 3 s. The myotonic run was terminated because over a span of seconds progressively more I_{Na} was slow-inactivated. A stable depolarized state, corresponding to paralysis, did not occur when the fast gating defects for T698M were combined with normal slow inactivation. These simulations show that the changes in slow inactivation we observed for T698M are sufficiently large to alter the muscle phenotype predicted by our model.

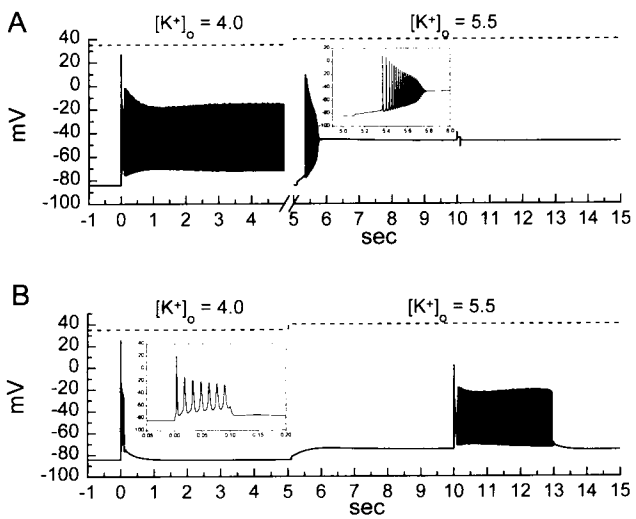

FIGURE 14 Myotonia and paralysis were enhanced by the defect in slow inactivation for T698M. Membrane potential is shown for a simulated muscle cell in response to a 100-ms current pulse (25 $\mu A/cm^2$) applied at $t = 0$, a step increase of extracellular $[K^+]$ from 4 to 5.5 mM at $t = 5$ s, and a second 100-ms current pulse (25 $\mu A/cm^2$) at $t = 10$ s. Simulated cells contained 50% WT and 50% T698M channels. (*A*) Simulated T698M channels had defects in activation, fast inactivation, and slow inactivation (see text for details). Current injection elicited prolonged myotonia. Resting potential was reset to −85 mV at $t = 5$ s, and the simulation was continued. Elevated $[K^+]_o$ depolarized the model cell to −46 mV, from which further action potentials could not be elicited. The inset shows the response to the step in $[K^+]_o$ on an expanded time scale. (*B*) Removal of the slow inactivation defect for T698M channels, while retaining the fast gating defects, reduced the propensity for myotonia or paralysis. Current injection and jump in extracellular $[K^+]$ were the same as in *A*. The inset shows the response on an expanded time scale for the current injection when $[K^+]_o = 4$ mM.

Based on the observed behavior of mutant Na channels and the quantitative predictions from our simulated muscle, we conclude that slow inactivation influences the propensity for myotonia and paralysis, but that a defect of slow inactivation is not a necessary condition for either. The two most common mutations found in association with HyperPP (T698M and M1585V) impair slow inactivation. Furthermore, the disruption of slow inactivation increases the tendency of defects in fast gating to cause stable depolarization and weakness (Figs. 12 and 13). Slow inactivation defects are not obligatory for the expression of symptoms, however, because other mutations associated with weakness (M1353V), myotonia (G1299E), or myotonia plus weakness (T1306M) have normal slow inactivation. Because normal Na channels are never completely slow-inactivated (Fig. 8), defects in fast gating (inactivation or activation) alone can produce perturbations in the equilibrium potential and thereby cause paralysis (Fig. 12). However, the degree of depolarization achieved with hyperkalemia, and therefore the likelihood of paralysis, is enhanced when there is also a defect in slow inactivation.

We thank Adriana Pechanova for assistance with tissue culture and preparation of plasmid DNA.

This work was supported by a postdoctoral fellowship from the Howard Hughes Medical Institute (LJH), the National Institutes of Health (AR42703 and NS07340), and the Cecil B. Day Co. (RHB). SCC is a Klingenstein Fellow and was supported by the Esther A. and Joseph Klingenstein Fund.

REFERENCES

Aldrich, R. W., and C. F. Stevens. 1987. Voltage-dependent gating of single sodium channels from mammalian neuroblastoma cells. *J. Neurosci.* 7:418–431.

Almers, W., P. R. Stanfield, and W. Stuhmer. 1983. Slow changes in currents through sodium channels in frog muscle membrane. *J. Physiol. (Lond.).* 339:253–271.

Balser, J. R., H. B. Nuss, N. Chiamvimonvat, M. T. Perez-Garcia, E. Marban, and G. F. Tomaselli. 1996. External pore residue mediates slow inactivation in μl rat skeletal muscle sodium channels. *J. Physiol. (Lond.).* 494:431–442.

Cannon, S. C. 1994a. A predilection for myotonia or paralysis based on different defects in Na channel inactivation. *J. Gen. Physiol.* 104:20a.

Cannon, S. C. 1994b. Slow sodium channel inactivation need not be disrupted in the pathogenesis of myotonia and periodic paralysis. *Biophys. J.* 66:543–544.

Cannon, S. C. 1996. Ion-channel defects and aberrant excitability in myotonia and periodic paralysis. *Trends Neurosci.* 19:3–10.

Cannon, S. C., R. H. Brown, Jr., and D. P. Corey. 1991. A sodium channel defect in hyperkalemic periodic paralysis: potassium-induced failure of inactivation. *Neuron.* 6:619–626.

Cannon, S. C., R. H. Brown, Jr., and D. P. Corey. 1993. Theoretical reconstruction of myotonia and paralysis caused by incomplete inactivation of sodium channels. *Biophys. J.* 65:270–288.

Cannon, S. C., L. J. Hayward, J. Beech, and R. H. Brown, Jr. 1995. Sodium channel inactivation is impaired in equine hyperkalemic periodic paralysis. *J. Neurophysiol.* 73:1892–1899.

Cannon, S. C., A. I. McClatchey, and J. F. Gusella. 1993. Modification of the Na+ current conducted by the rat skeletal muscle alpha subunit by coexpression with a human brain beta subunit. *Pflugers Arch.* 423: 155–157.

Cannon, S. C., and S. M. Strittmatter. 1993. Functional expression of sodium channel mutations identified in families with periodic paralysis. *Neuron.* 10:317–326.

Chahine, M., A. L. George, Jr., M. Zhou, S. Ji, W. Sun, R. L. Barchi, and R. Horn. 1994. Sodium channel mutations in paramyotonia congenita uncouple inactivation from activation. *Neuron.* 12:281–294.

Cummins, T. R., and F. J. Sigworth. 1996. Impaired slow inactivation in mutant sodium channels. *Biophys. J.* 71:227–236.

Cummins, T. R., J. Zhou, F. J. Sigworth, C. Ukomadu, M. Stephan, L. J. Ptacek, and W. S. Agnew. 1993. Functional consequences of a Na^+ channel mutation causing hyperkalemic periodic paralysis. *Neuron.* 10: 667–678.

Featherstone, D. E., J. E. Richmond, and P. C. Ruben. 1996. Interaction between fast and slow inactivation in SkM1 sodium channels. *Biophys. J.* 71:3098–3109.

Hayward, L. J., R. H. Brown, Jr., and S. C. Cannon. 1996. Inactivation defects caused by myotonia-associated mutations in the sodium channel III–IV linker. *J. Gen. Physiol.* 107:559–576.

Jurman, M. E., L. M. Boland, Y. Liu, and G. Yellen. 1994. Visual identification of individual transfected cells for electrophysiology using antibody-coated beads. *Biotechniques.* 17:876–881.

Lehmann-Horn, F., R. Rudel, and K. Ricker. 1993. Non-dystrophic myotonias and periodic paralyses. A European Neuromuscular Center Workshop held 4–6 October 1992, Ulm, Germany. *Neuromuscul. Disord.* 3:161–168.

Lerche, H., R. Heine, U. Pika, A. L. George, Jr., N. Mitrovic, M. Browatzki, T. Weiss, M. Rivet-Bastide, C. Franke, M. Lomonaco, K. Ricker, and F. Lehmann-Horn. 1993. Human sodium channel myotonia: slowed channel inactivation due to substitutions for a glycine within the III–IV linker. *J. Physiol. (Lond.).* 470:13–22.

Lerche, H., N. Mitrovic, V. Dubowitz, and F. Lehmann-Horn. 1996. Paramyotonia congenita: the R1448P Na^+ channel mutation in adult human skeletal muscle. *Ann. Neurol.* 39:599–608.

McClatchey, A. I., S. C. Cannon, S. A. Slaugenhaupt, and J. F. Gusella. 1993. The cloning and expression of a sodium channel beta 1-subunit cDNA from human brain. *Hum. Mol. Genet.* 2:745–749.

Mitrovic, N., A. L. George, Jr., R. Heine, S. Wagner, U. Pika, U. Hartlaub, M. Zhou, H. Lerche, C. Fahlke, and F. Lehmann-Horn. 1994. K(+)-aggravated myotonia: destabilization of the inactivated state of the human muscle Na^+ channel by the V1589 M mutation. *J. Physiol. (Lond.).* 478:395–402.

Mitrovic, N., A. L. George, Jr., H. Lerche, S. Wagner, C. Fahlke, and F. Lehmann-Horn. 1995. Different effects on gating of three myotonia-causing mutations in the inactivation gate of the human muscle sodium channel. *J. Physiol. (Lond.).* 487:107–114.

Ptacek, L. J., L. Gouw, H. Kwiecinski, P. McManis, J. R. Mendell, R. J. Barohn, A. L. George, Jr., R. L. Barchi, M. Robertson, and M. F. Leppert. 1993. Sodium channel mutations in paramyotonia congenita and hyperkalemic periodic paralysis. *Ann. Neurol.* 33:300–307.

Rudy, B. 1978. Slow inactivation of the sodium conductance in squid giant axons. Pronase resistance. *J. Physiol. (Lond.).* 283:1–21.

Ruff, R. L. 1994. Slow Na^+ channel inactivation must be disrupted to evoke prolonged depolarization-induced paralysis. *Biophys. J.* 66: 542–545.

Ruff, R. L., L. Simoncini, and W. Stuhmer. 1987. Comparison between slow sodium channel inactivation in rat slow- and fast-twitch muscle. *J. Physiol. (Lond.).* 383:339–348.

Sambrook, J., E. F. Fritsch, and T. Maniatis. 1989. Molecular Cloning: A Laboratory Manual. Cold Spring Harbor Laboratory, Cold Spring Harbor, NY.

Simoncini, L., and W. Stühmer. 1987. Slow sodium channel inactivation in rat fast-twitch muscle. *J. Physiol. (Lond.).* 383:327–337.

Tahmoush, A. J., K. L. Schaller, P. Zhang, T. Hyslop, T. Heiman-Patterson, and J. H. Caldwell. 1994. Muscle sodium channel inactivation defect in paramyotonia congenita with the thr1313 met mutation. *Neuromuscul. Disord.* 4:447–454.

Trimmer, J. S., S. S. Cooperman, S. A. Tomiko, J. Y. Zhou, S. M. Crean, M. B. Boyle, R. G. Kallen, Z. H. Sheng, R. L. Barchi, F. J. Sigworth, R. H. Goodman, W. S. Agnew, and G. Mandel. 1989. Primary structure and functional expression of a mammalian skeletal muscle sodium channel. *Neuron.* 3:33–49.

Ukomadu, C., J. Zhou, F. J. Sigworth, and W. S. Agnew. 1992. μl Na^+ channels expressed transiently in human embryonic kidney cells: biochemical and biophysical properties. *Neuron.* 8:663–676.

Valenzuela, C., and P. B. Bennett, Jr. 1994. Gating of cardiac Na^+ channels in excised membrane patches after modification by alpha-chymotrypsin. *Biophys. J.* 67:161–171.

West, J. W., D. E. Patton, T. Scheuer, Y. Wang, A. L. Goldin, and W. A. Catterall. 1992. A cluster of hydrophobic amino acid residues required for fast Na(+)-channel inactivation. *Proc. Natl. Acad. Sci. USA.* 89: 10910–10914.

Yang, N., S. Ji, M. Zhou, L. J. Ptacek, R. L. Barchi, R. Horn, and A. L. George, Jr. 1994. Sodium channel mutations in paramyotonia congenita exhibit similar biophysical phenotypes in vitro. *Proc. Natl. Acad. Sci. USA.* 91:12785–12789.